31st Annual International Conference of the IEEE EMBS
Minneapolis, Minnesota, USA, September 2-6, 2009

Animal and Human Imaging Experiments in Magnetic Resonance Electrical Impedance Tomography (MREIT)

Eung Je Woo, *Member, IEEE*

***Abstract*—Cross-sectional imaging of an electrical conductivity distribution inside the human body has been an active research topic in the field of impedance imaging. This paper describes the recent progress in Magnetic Resonance Electrical Impedance Tomography (MREIT) where conductivity imaging with a spatial resolution of a few mm is pursued. After the early studies on its theory and image reconstruction algorithms, MREIT has reached the stage of *in vivo* animal and human imaging experiments. After reviewing latest MREIT imaging experiments, we discuss several technical challenges to be addressed in the future work.**

I. Introduction

Electrical conductivity values of biological tissues may provide valuable diagnostic information that are not readily available from existing imaging modalities based on X-ray, γ-ray, magnetic resonance, and ultrasound. Magnetic Resonance Electrical Impedance Tomography (MREIT) is a lately developed impedance imaging method that is expected to provide cross-sectional conductivity images of the human body with a spatial resolution of a few mm [1-10].

Injected current into an electrically conducting object including the human body induces internal distributions of current density, voltage, and magnetic flux density. In MREIT, we use an MRI scanner with its main magnetic field pointing the z-direction to measure the induced magnetic flux density B_z that is the z-directional component. Multiple injection currents using at least two pairs of electrodes are adopted to produce multiple B_z data. One may add a few voltage measurements to the data set.

We apply a conductivity image reconstruction algorithm to the data set and produce multi-slice cross-sectional images of a conductivity distribution inside a chosen three-dimensional imaging domain. Following the review paper on MREIT [10], this paper summarizes the latest results of MREIT including animal and human imaging experiments.

Though these results demonstrated the feasibility of MREIT as a high-resolution conductivity imaging modality, there still exist a few technical challenges. We will briefly discuss what should be done in future studies to make the MREIT technique applicable to clinical settings.

Manuscript received April 7, 2009. This work was supported by the SRC/ERC program (R11-2002-103) of MOST/KOSEF.

E. J. Woo is with the Department of Biomedical Engineering, College of Electronics and Information, Kyung Hee University, 1 Seocheon-dong, Giheung-gu, Yongin-si, Gyeonggi-do, 446-701, Korea (phone: +82-21-201-2538; fax: +82-31-201-2378; e-mail: ejwoo@khu.ac.kr).

II. Methods

A. MREIT System

Imaging experiments in MREIT are performed inside an MRI scanner that is equipped with a constant current source. Fig. 1 shows a 3 T MRI scanner and an MREIT current source used in the Impedance Imaging Research Center (IIRC, http://iirc.khu.ac.kr). We may employ a conventional spin-echo pulse sequence and inject currents in a synchronized way as illustrated in Fig. 2.

(a) (b)

Fig. 1. (a) 3 T MRI scanner and (b) MREIT current source at IIRC..

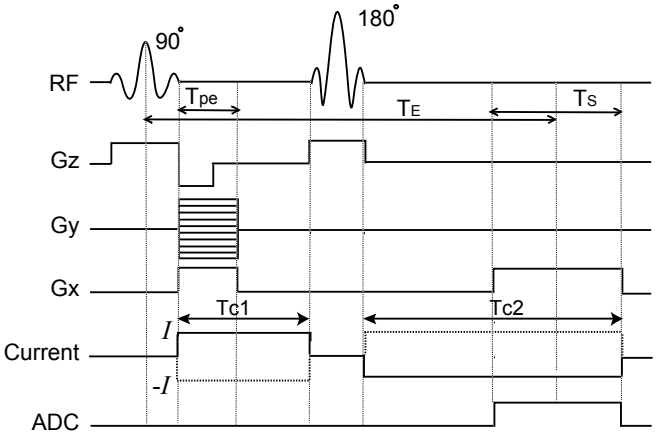

Fig. 2. MREIT pulse sequence [11] to acquire B_z data subject to an injection current.

Fig. 3(a) and (b) show a recessed and a carbon-hydrogel electrode used in most MREIT experiments. In both types, nonmagnetic materials such as the copper or carbon are used as electrodes. In order to alleviate the technical problem related with RF shielding artifacts from a highly conductive material, the thin conductive electrode is moved away from the skin by a layer of appropriate conductive gel. Since the carbon-hydrogel electrode offers more advantages including

its large contact area, flexibility and good contact, most recent studies adopted it [12-15].

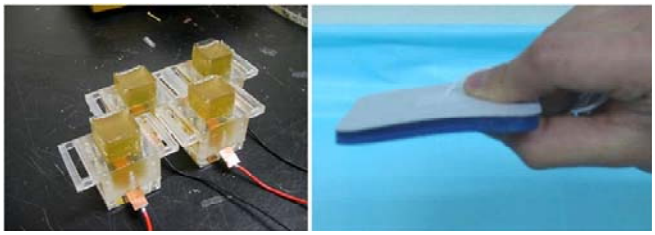

(a) (b)

Fig. 3. (a) Rigid recessed electrode and (b) flexible carbon-hydrogel electrode.

B. Experimental Procedure

Inside the bore of the MRI scanner, we place the imaging object with four electrodes attached around a chosen imaging region as shown in Fig. 4. This allows us to inject currents I_1 and I_2 along two different directions. For an isotropic (or equivalent isotropic) conductivity image reconstruction [xxx, xxx], we get induced magnetic flux densities $B_{z,1}$ and $B_{z,2}$ corresponding to I_1 and I_2, respectively. Examples of imaging parameters are as follows: TR/TE = 1200/30 ms, FOV = 220×220 mm^2, slice thickness = 4 mm, NEX = 10, matrix size = 128×128, number of slices = 8, and total imaging time = 100 min.

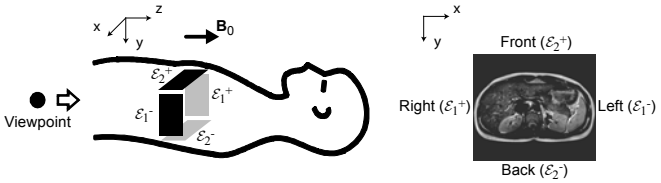

Fig. 4. Experimental setup in MREIT.

C. Conductivity Image Reconstruction

Though there are several conductivity image reconstruction algorithms, we found that the harmonic B_z algorithm [6,7,16] is most suitable to produced scaled conductivity images providing contrast information. Since the harmonic B_z algorithm assumes an isotropic conductivity distribution, reconstructed images must be interpreted as equivalent isotropic conductivity images [13].

Lately, the MREIT group at IIRC developed an MREIT software package with an efficient graphical user interface. They called it CoReHA which stands for conductivity reconstructor using harmonic algorithms. As shown in Fig. 5, it offers various computational tools including preprocessing of MREIT data, image segmentation for extraction of boundary geometry, electrode shape and positions, denoising, harmonic inpainting, conductivity image reconstruction, post-processing and visualization. In this paper, we present conductivity images of animal and human subjects reconstructed by using CoReHA.

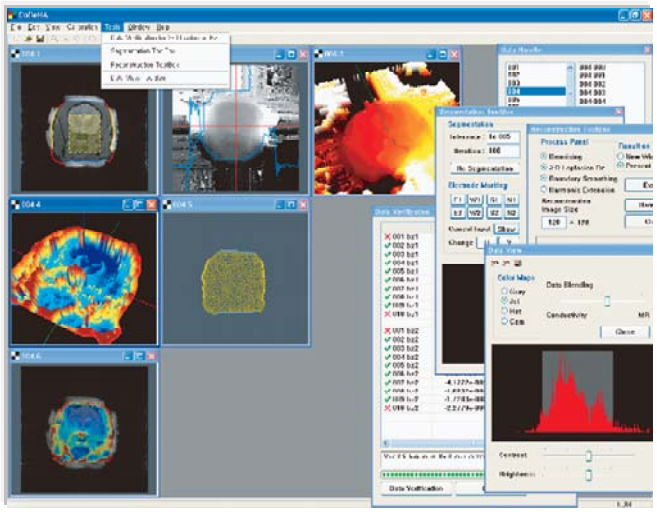

Fig. 5. MREIT software package, CoReHA.

III. Results

A. Animal Images

Fig. 6 and 7 show postmortem and *in vivo* canine brain images, respectively, from three consecutive imaging slices [13, 14]. Different brain tissues of white matter, gray matter, and limbic areas are distinguished in reconstructed conductivity images. Postmortem images exhibit much higher SNR compared with *in vivo* images primarily due to the high amplitude of injection current (40 mA in postmortem experiment versus 5 mA in *in vivo* experiment). Fig. 8 compares conductivity images of the brain only with those of the entire canine head.

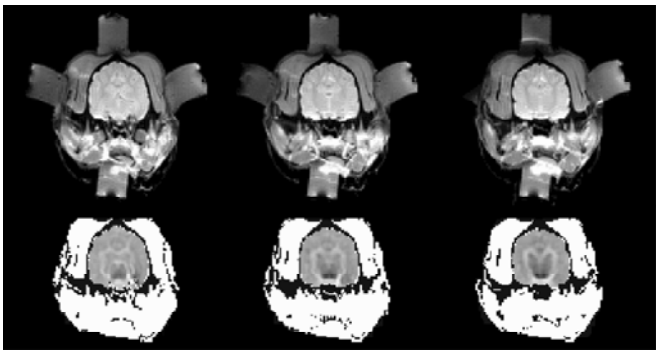

Fig. 6. Postmortem canine brain images using 40 mA injection currents. Top and bottom rows are MR magnitude and conductivity images, respectively [13].

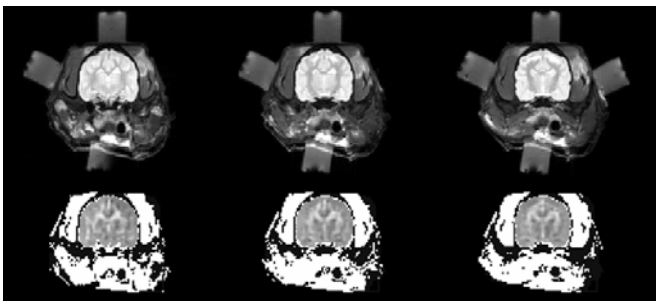

Fig. 7. *In vivo* canine brain images using 5 mA injection currents. Top and bottom rows are MR magnitude and conductivity images, respectively [14].

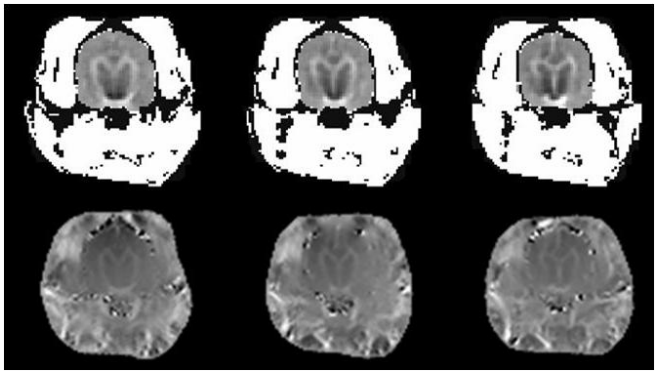

Fig. 8. Top and bottom rows are conductivity images of the canine brain only and the entire canine head, respectively.

Fig. 9 and 10 show postmortem canine abdomen and pelvis images. In Fig. 9, the kidney, urethra, spleen, liver, spinal cord, and small intestines are distinguished in reconstructed conductivity images. In Fig. 10, the prostate grand, rectum, sacrum, and medial gluteus medius are distinguished in reconstructed conductivity images.

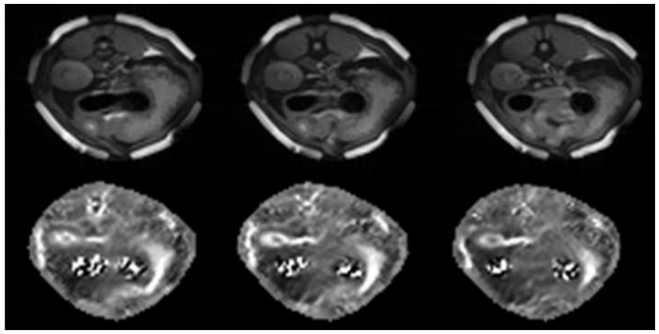

Fig. 9. Postmortem canine abdomen images. Top and bottom rows are MR magnitude and conductivity images, respectively.

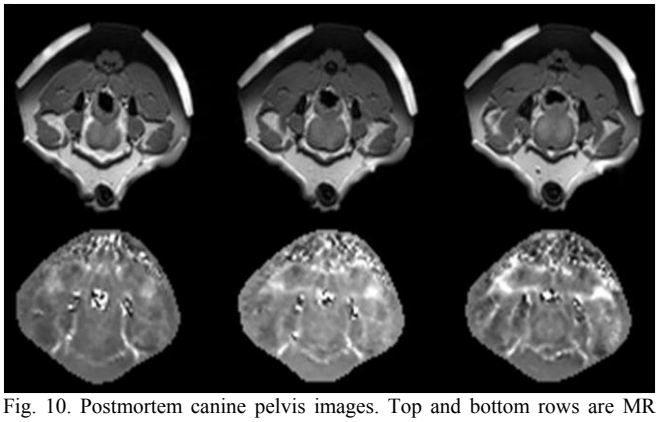

Fig. 10. Postmortem canine pelvis images. Top and bottom rows are MR magnitude and conductivity images, respectively.

Fig. 11 shows postmortem canine chest images. We can observe that reconstructed conductivity images inside local regions of MR signal void are noisy. This is particularly apparent in the lungs of the chest images in Fig. 11.

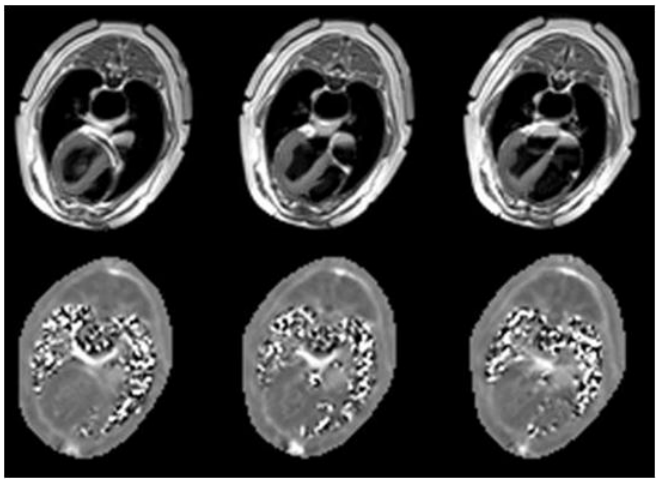

Fig. 11. Postmortem canine chest images. Top and bottom rows are MR magnitude and conductivity images, respectively.

B. Human Images

Fig. 12 and 13 are *in vivo* images of the human leg from a male and female subject, respectively. We can distinguish the skeletal muscle, adipose tissue, crural fascia, intermuscular septum, and yellow marrow [15].

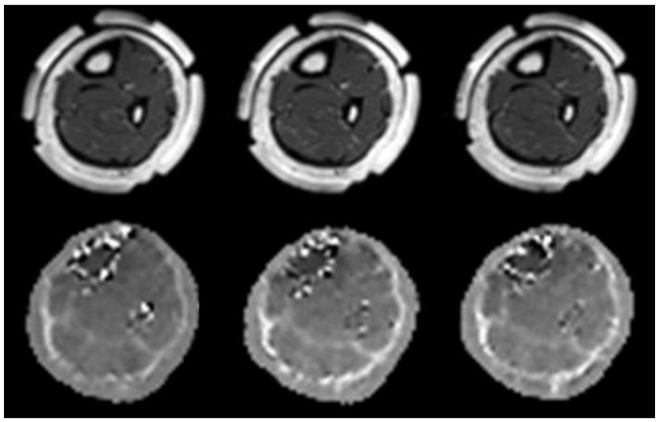

Fig. 12. *In vivo* human leg images (male). Top and bottom rows are MR magnitude and conductivity images, respectively [15].

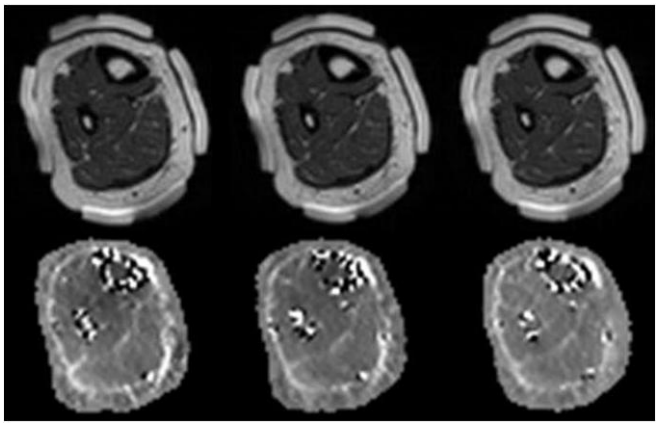

Fig. 13. *In vivo* human leg images (female). Top and bottom rows are MR magnitude and conductivity images, respectively [15].

IV. Discussion and Conclusion

Even though MREIT is capable of producing a conductivity image in absolute conductivity values, practical implementation so far provides a scaled conductivity image with contrast information only. Interpretation of such a scaled conductivity image requires further investigation using numerous animal models. We plan to undertake imaging experiments for characterization of pathologic tissues and organs.

In terms of the technical aspect of this new imaging modality, experimental results so far have revealed technical challenges that need to be addressed. First, MR signal void or low SNR in some internal local regions result in a noisy conductivity image. We need to develop a ramp-preserving denoising method that preserves deflections of B_z signal related with a local conductivity contrast. For the case where we can safely assume a constant conductivity in a local region of MR signal void, we can utilize an inpainting technique.

Second, more sophisticated implementation of the harmonic B_z algorithm or its variants is necessary to improve the image quality [16]. Hybrid algorithms with *a priori* structural information from an MR magnitude image should also be pursued. Third, we need to investigate effects of tissue anisotropy and come up with a more thorough understanding of a reconstructed equivalent isotropic conductivity image. Enhancing the SNR in measured B_z data and utilizing more than two injection currents, it would be desirable to develop a practically implementable method to produce an anisotropic conductivity image.

Fourth, we are limited by the amount of injection current primarily for the safety reason as any other impedance imaging methods based on injection currents. Depending on a specific application, the amount may also be limited by any physiological effect that must be refrained within a certain level. We should provide a guideline for the current amplitude and width. This, however, is not a trivial task since we should consider its relation with an achievable image quality.

Fifth, the image quality in MREIT is basically dependent upon the SNR in measured B_z data. We should devise an optimal data collection scheme considering the performance of an adopted MRI scanner and RF coils, voxel size, and pulse sequence. We suggest MREIT studies using a high-performance parallel MRI scanner and specialized pulse sequence.

Acknowledgment

This work was supported by the SRC/ERC program (R11-2002-103) of MOST/KOSEF.

References

[1] N. Zhang, *Electrical Impedance Tomography based on Current Density Imaging*, MS Thesis, Dept. of Elec. Eng., Univ. of Toronto, Toronto, Canada, 1992.

[2] E. J. Woo, S. Y. Lee, and C. W. Mun, "Impedance tomography using internal current density distribution measured by nuclear magnetic resonance," *SPIE*, vol. 2299, pp. 377-385, 1994.

[3] O. Birgul and Y. Z. Ider, "Use of the magnetic field generated by the internal distribution of injected currents for electrical impedance tomography," *Proc. IXth Int. Conf. Elec. Bio-Impedance*, Heidelberg, Germany, pp. 418-419, 1995.

[4] Y. Z. Ider and O. Birgul, "Use of the magnetic field generated by the internal distribution of injected currents for Electrical Impedance Tomography (MR-EIT)," *Elektrik*, vol. 6, pp. 215-225, 1998.

[5] O. Kwon, E. J. Woo, J. R. Yoon, and J. K. Seo, "Magnetic resonance electrical impedance tomography (MREIT): simulation study of J-substitution algorithm," *IEEE Trans. Biomed. Eng.*, vol. 48, pp. 160-167, 2002.

[6] J. K. Seo, J. R. Yoon, E. J. Woo, and O. Kwon, "Reconstruction of conductivity and current density images using only one component of magnetic field measurements," *IEEE Trans. Biomed. Eng.*, vol. 50, pp. 1121-1124, 2003.

[7] S. H. Oh, B. I. Lee, E. J. Woo, S. Y. Lee, M. H. Cho, O. Kwon, and J. K. Seo, "Conductivity and current density image reconstruction using harmonic B_z algorithm in magnetic resonance electrical impedance tomography," *Phys. Med. Biol.*, vol. 48, pp. 3101-3116, 2003.

[8] O. Birgul, B. M. Eyuboglu, and Y. Z. Ider, "Experimental results for 2D magnetic resonance electrical impedance tomography (MREIT) using magnetic flux density in one direction," *Phys. Med. Biol.*, vol. 48, pp. 3485-3504, 2003.

[9] E. J. Woo, J. K. Seo, and S. Y. Lee, "*Magnetic resonance electrical impedance tomography (MREIT)*," in *Electrical Impedance Tomography: Methods, History and Applications*, D. Holder, Ed., Bristol, UK: IOP Publishing, 2005.

[10] E. J. Woo and J. K. Seo, "Magnetic resonance electrical impedance tomography (MREIT) for high-resolution conductivity imaging," *Physiol. Meas.*, vol. 29, pp. R1-R26, 2008.

[11] C. Park, B. I. Lee, O. Kwon, and E. J. Woo, "Measurement of induced magnetic flux density using injection current nonlinear encoding (ICNE) in MREIT," *Physiol. Meas.*, vol. 28, pp. 117-127, 2006.

[12] S. H. Oh, B. I. Lee, E. J. Woo, S. Y. Lee, T. S. Kim, O. Kwon, and J. K. Seo, "Electrical conductivity images of biological tissue phantoms in MREIT," *Physiol. Meas*., vol. 26, pp. S279-S288, 2005.

[13] H. J. Kim, B. I. Lee, Y. T. Kim, B. I. Lee, E. J. Woo, J. K. Seo, S. Y. lee, O. Kwon, C. Park, B. T. Kang, and H. M. Park, "Conductivity imaging of canine brain using a 3 T MREIT system: postmortem experiments," *Physiol. Meas.*, vol. 28, pp. 1341-1353, 2007.

[14] H. J. Kim, T. I. Oh, Y. Cho, Y. T. Kim, B. T. Kang, H. M. Park, S. Y. Lee, J. K. Seo, and E. J. Woo, "*In vivo* electrical conductivity imaging of a canine brain using a 3 T MREIT system," *Physiol. Meas.*, vol. 29, pp. 1145-1155, 2008.

[15] H. J. Kim, Y. T. Kim, A. S. Minhas, W. C. Jeong, E. J. Woo, J. K. Seo, and O J. Kwon, "*In vivo* high-resolution conductivity imaging of the human leg using MREIT: the first human experiment," *IEEE Trans. Med. Imag.*, in press.

[16] J. K. Seo, S. W. Kim, S. Kim, J. J. Liu, E. J. Woo, K. Jeon, and C-O. Lee, "Local harmonic Bz algorithm with domain decomposition in MREIT: computer simulation study," *IEEE Trans. Med. Imag.*, vol. 27, pp. 1754-1761, 2008.